SLIP-FLOW OVER LUBRICATED SURFACES

Stian Solbakken, Helge I. Andersson
Department of Energy and Process Engineering,
Norwegian University of Science and Technology (NTNU)
7491 Trondheim, Norway
stian.solbakken@mtf.ntnu.no, helge.i.andersson@mtf.ntnu.no

Jens Neumann
Institut für Strömungsmechanik und Aerodynamik,
Universität der Bundeswehr München
85577 Neubiberg, Germany
jens.neumann@unibw-muenchen.de

ABSTRACT

A direct numerical simulation (DNS) of a lubricated turbulent channel flow is performed. The lubricating film, present at both channel walls, is replaced by a new set of dynamic slip-flow boundary conditions imposed at the planar film-fluid interface. The proposed slip-flow boundary conditions are verified against a simulation where both the lubricating film and the bulk fluid have been solved within the DNS approach. Both turbulence statistics and instantaneous near-wall vortical structures are satisfactorily reproduced by the slip-flow boundary conditions.

INTRODUCTION

Turbulent flows in the presence of lubricated surfaces are often encountered in engineering applications, and such flows represent an interesting example of the coupled motion of two fluids separated by an interface. The modelling of the moving interface is complicated (e.g. Scardovelli and Zaleski, 1999), even though the problem is in general dealt with assuming only continuity of velocity components as well as stresses across the interface. Solbakken *et al.* (2002) performed a direct numerical simulation of a lubricated turbulent channel flow where they simplified the problem by prescribing a planar impermeable interface between the lubricant at the wall and the bulk flow. A direct numerical simulation of both the lubricating layer and the bulk fluid will undoubtedly give the most realistic solution of the problem, but the limitations of numerical techniques make it difficult to include a freely deforming interface. An accurate numerical solution would also require either a very fine computational mesh in the neighbourhood of the interface or an adaptive grid, which have to be adjusted at each time-step. The computational cost and numerical difficulties make such simulations hard to accomplish. One way of overcoming these difficulties is to replace the actual interface by a smooth boundary and introduce a dynamic slip boundary condition at the interface between the two fluids.

The idea of a slip-flow boundary condition is not new and was first introduced by Navier (1823) during the long debate on whether a fluid can slide over a solid surface. Navier's proposed boundary condition assumes that the velocity u at a solid surface is proportional to the shear rate at the surface, i.e.

$$u = \beta \frac{\partial u}{\partial y} , \qquad (1)$$

where β is the slip length or slip coefficient. If $\beta = 0$ the generally assumed no-slip boundary condition is obtained. Since the no-slip condition appears to be valid at macroscale, β must be relatively small for Navier's hypothesis to hold. It is generally accepted that the continuum model is valid as long as $Kn < 10^{-1}$ (Knudsen number) and the motion of a Newtonian fluid is then described by the Navier-Stokes equations. But in the range $10^{-3} < Kn < 10^{-1}$ the no-slip condition at solid surfaces is not valid and is in fact replaced by slip-flow conditions (Gad-el-Hak, 1999).

The Navier condition was first invoked in the context of lubrication by Greenspan (1978). Shortly after Joseph (1980) derived an analytical slip-flow condition for a lubricated surface in which the velocity gradient is proportional to the square of the velocity component along the interface. By assuming a very thin lubricating film in which lubrication theory applies, and by neglecting the effect of the pressure gradient, he derived the following slip-flow condition in the streamwise (x) direction

$$\frac{\partial u}{\partial y} = \frac{\mu_l u^2}{2\mu_b Q} , \qquad (2)$$

where μ_l/μ_b is the ratio of viscosity of the lubricating fluid to the viscosity of the bulk fluid and Q is the constant volumetric flow rate per unit width in the lubricating film. If the film is sufficiently thin Joseph (1980) suggests that the effect of the thin lubrication layer may be accommodated by changing the boundary condition at the solid surface according to eq. (2). More recently Miksis and Davis (1994) derived a more general slip boundary condition for a film-covered rough surface in the limit of small-amplitude roughness and thin lubricating films.

The objective of the present study is to suggest and apply a proper set of dynamic boundary conditions at the interface between a turbulent channel flow and a thin lubricating film. The hypothesis is that such slip boundary conditions are able to mimic interfacial motions present at the film-bulk fluid interface. The lubricating film can then be accomodated by the slip-flow boundary conditions, making the solution of the velocity field inside the film unnecessary. It is important to apply dynamic boundary conditions capable of generating both spatial and temporal variations when turbulence is considered. Furthermore, it is essential that the proposed slip-flow conditions result in quantitatively good results for the mean field and the turbulence statistics. But it would

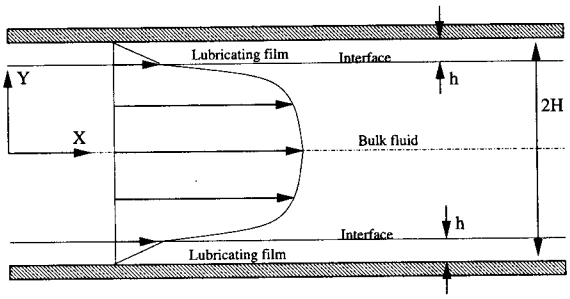

Figure 1: Sketch of the flow geometry. The two solid lines at $y = \pm(H - h)$ are the interface where the slip-flow boundary conditions eqs. (2) and (3) are applied.

also be favourable if the use of slip-flow conditions reproduce realistic instantaneous interfacial motions in such a way that the near-interface stress-producing coherent structures remain reasonable.

We propose to use Joseph's (1980) slip-flow condition as a dynamic boundary condition at the interface in the streamwise direction. Originally this relation was developed for $2 - D$ situations, i.e. laminar flow. But the slip-flow condition (2) should also be valid for turbulent flows since it is only dependent on material parameters and not on flow characteristics in the bulk fluid. In the case of turbulent flow a spanwise slip condition is also required. A dynamic slip-flow boundary condition with zero mean velocity at the interface is neccessary, and we propose to use the following drag-flow approximation in the spanwise (z) direction:

$$\frac{\partial w}{\partial y} = \frac{\mu_l w}{\mu_b h} , \qquad (3)$$

where h is the lubricating film thickness. Equations (2) and (3) have been implemented as new boundary conditions in the computer code MGLET developed for DNS and LES in complex geometries.

A similar approach was successfully used by Hahn *et al.* (2002) in their direct numerical simulations of turbulent channel flow with permeable walls. They used an extended version of Beavers and Joseph's (1967) slip-flow boundary condition at the interface between a permeable block and and a laminar channel flow.

NUMERICAL APPROACH AND SIMULATION OVERVIEW

A direct numerical simulation (DNS) of a pressure-driven lubricated channel flow is performed. The lubricating film present at both channel walls is not handled within the DNS approach, but is instead accommodated for by the slip-flow boundary conditions eqs. (2) and (3) imposed at the interface between the bulk-fluid and the lubricant. Only the flow field in the bulk fluid and the interfacial velocities between the bulk-fluid and the lubricant are computed. The previous simulation by Solbakken *et al.* (2002) is almost identical to the present, except for the treatment of the lubricating film, which in Solbakken *et al.* (2002) was resolved on the computational mesh and solved within the DNS approach. The present simulation is thus a simplification of the more accurate investigation by Solbakken *et al.* (2002).

A side view of the channel flow geometry and co-ordinate system is shown in fig. 1. Both channel walls are covered with a lubricating film of thickness $h = H/18$ (H is channel half height), having a kinematic viscosity twice that of the bulk fluid ($\nu_l = 2\nu_b$), i.e. identical to Solbakken *et al.* (2002). The interface is maintained flat by imposing the impermeability condition $v_{wall-normal} = 0$. A global Reynolds number is commonly defined as $Re_\tau = u_\tau H/\nu_b = 180$ where u_τ is the wall friction velocity. Here, it is more appropriate to define a Reynolds number for the bulk flow based on the interfacial friction velocity $Re_b = (H - h)u_{\tau i}/\nu_b \approx 165$ where the interfacial friction velocity can be expressed as $u_{\tau i} = u_\tau(1 - h/H)^{0.5}$. The computational domain in the streamwise (x), wall-normal (y) and spanwise (z) directions is $4\pi H \times 2(H - h) \times 2\pi H$, and the corresponding number of grid cells are $192 \times 172 \times 192$. The computational mesh is non-uniform in the y-direction, the grid point next to the interface being at $y^+ = 0.5$. The mesh is identical to the part of the mesh used for resolving the bulk-flow in Solbakken *et al.* (2002). Slip-flow boundary conditions, eqs. (2) and (3), and impermeability, $v_{wall-normal} = 0$, are applied at the two interfaces while periodicity is used in the two homogenous directions.

The computer code MGLET (Manhart *et al.*, 2001, Orellano and Wengle, 2000) used in the present study, is based on a finite volume formulation of the Navier-Stokes equations on a staggered Cartesian non-equidistant mesh. The spatial discretization is of second-order central for the convective and diffusive terms. An explicit version of the projection method together with a second-order Leapfrog scheme is used for the time integration. The resulting Poisson equation is solved by an iterative procedure accelerated by a multigrid method.

The proposed boundary conditions (2) and (3) are implemented as dynamic boundary conditions utilizing ordinary ghost cells outside the computational domain. The boundary conditions are updated in the ghost cells for each new time step $n+1$ by using the solution in the bulk flow from the previous time step n. Consider the discretization of Navier's slip boundary condition (1) as an example:

$$u = \beta\frac{\partial u}{\partial y} \Longrightarrow \frac{1}{2}(u_0^{n+1} + u_1^n) = \beta\frac{u_1^n - u_0^{n+1}}{\Delta y} , \qquad (4)$$

where u_0 and u_1 are the velocities in the ghost cell and in the neighbour cell inside the computational domain, respectively, and Δy is the distance between the two. u_0 and u_1 are equally spaced from the boundary. u_0^{n+1} can then be expressed explicitly as a function of u_1^n:

$$u_0^{n+1} = u_1^n\frac{2\beta/\Delta y - 1}{1 + 2\beta/\Delta y} . \qquad (5)$$

An iterative procedure in which u_0 is continously updated would be slightly more accurate, but no major errors are introduced by the present scheme if the time-step is kept sufficiently small.

The lubricating film that separates the bulk-fluid from the rigid wall is thus accommodated by eqs. (2) and (3), applied at the interface, and the velocity field within the film is therefore not computed. But in order to calculate the wall friction necessary to balance the imposed pressure gradient, also the flow field in the film is needed. This problem is simply solved by assuming a linear velocity profile inside the film, and then the velocity gradient at the interface can be used when calculating τ_{wall}. The assumption of a linear velocity profile can also be used in order to calculate the volumetric flow rate Q inside the film, which is needed as an input parameter in the streamwise slip-flow boundary condition (2). However, the present investigation uses Q calculated from the DNS of Solbakken *et al.* (2002), which is 3.5% larger than what is obtained by assuming a linear velocity profile.

INTERFACIAL BEHAVIOUR

The outcome of an accurate direct numerical simulation of a lubricated turbulent channel flow using the proposed slip-flow boundary conditions (2) and (3) depends highly on the ability of these conditions to mimic real interfacial motions. In order to examine the validity of the proposed boundary conditions, results from the present simulation using eqs. (2) and (3) are compared with data extracted from the simulation by Solbakken *et al.* (2002) where both the lubricating film and the bulk fluid were solved simultaneously within the DNS approach. This section focuses on the interfacial velocities and velocity gradients and their instantaneous distributions.

Figures 2 and 3 are scatter plots of u vs. $\partial u/\partial y$ and w vs. $\partial w/\partial y$, respectively, at the interface between the lubricating film and the bulk fluid. The data are sampled from instantaneous flow fields from the simulation by Solbakken *et al.* (2002). Note that the velocity gradients are evaluated in the bulk flow. Also included in these figures are the two proposed boundary conditions eqs. (2) and (3) in figs. 2 and 3, respectively. A scatter plot of instantaneous data from the present simulation (not shown here) showed a perfect conformity with eqs. (2) and (3), which thus verifies the implementation of these in the computer code MGLET.

The scatter plot of $u_{interface}$ vs. $\partial u/\partial y_{interface}$ in fig. 2 shows good agreement with the streamwise slip-flow condition (2) proposed by Joseph (1980). The fairly large scattering of the instantaneous data reflects the higher degree of freedom present at the interface in the simulation by Solbakken *et al.* (2002) compared to the present one. The streamwise slip-flow condition eq. (2) slightly underpredicts the shear-rate at low interfacial velocities, whereas the interfacial shear-rate is somewhat too large at high velocities. It is promising that the mean value of the scatter plot (the circle in fig. 2) collapses with Joseph's (1980) slip-flow boundary condition. Figure 3 reveals that the scatter plot of $w_{interface}$ vs. $\partial w/\partial y_{interface}$ agrees satisfactorily with the proposed slip boundary condition, eq. (3), in the spanwise direction. The mean value of the scattered data shows a perfect match with eq. (3). However, the instantaneous data from Solbakken *et al.* (2002) suggest that the slope of eq. (3) is too small, which inevitably will result in either too large velocity fluctuations or too small velocity gradient fluctuations.

Probability density functions (PDFs) are constructed from the instantaneous data shown in the scatter plots in figs. 2 and 3 and from the corresponding instantaneous data from the present investigation. Figure 4 shows the PDFs of both u and $\partial u/\partial y$ at the interface. The PDFs of $u_{interface}$ in fig. 4(a) clearly show that eq. (2) is capable of generating a distribution that is practically identical with the distribution from Solbakken *et al.* (2002), which is assumed to be correct. It is promising that the mean value of $u_{interface}$ deviates by less than 1% from Solbakken *et al.* (2002). However, the distribution of $\partial u/\partial y_{interface}$ shows a distinct deviation from Solbakken *et al.* (2002). The data sampled from the present simulation are somewhat more widespread. This will obviously have a major effect on the rms-value of the spanwise component of the vorticity fluctuations at the interface since $|\omega_z|_{interface} \equiv \partial u/\partial y_{interface}$. But the mean value of $\partial u/\partial y_{interface}$ is identical to that in Solbakken *et al.* (2002), which is inevitable since this is fixed by the imposed pressure gradient. The PDFs of $w_{interface}$ and $\partial w/\partial y_{interface}$ in fig. 5 reveal a somewhat similar behaviour. But now the spanwise velocity $w_{interface}$

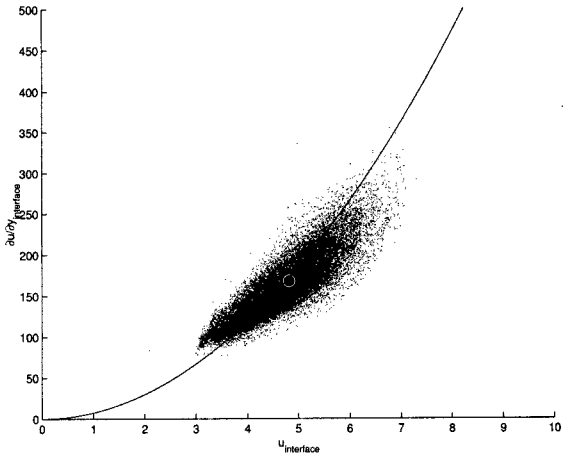

Figure 2: Scatter plot of u vs. $\partial u/\partial y$ at the interface from Solbakken *et al.* (2002). The circle is the mean value of the scatter plot and the solid line is eq. (2).

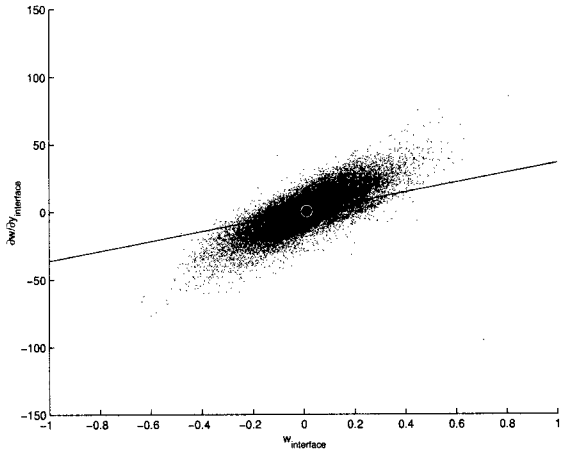

Figure 3: Scatter plot of w vs. $\partial w/\partial y$ at the interface from Solbakken *et al.* (2002). The circle is the mean value of the scatter plot and the solid line is eq. (3).

distribution is too widespread, while the distribution of the velocity gradient $\partial w/\partial y_{interface}$ is practically the same as in Solbakken *et al.* (2002). The PDF of $w_{interface}$ is too flat and accordingly the standard deviation will be too large. Remember that the standard deviation equals the rms-value of the fluctuations (turbulence intensity). The mean values of both $w_{interface}$ and $\partial w/\partial y_{interface}$ are essentially zero as expected for symmetry reasons.

MEAN FIELD AND TURBULENCE STATISTICS

The statistical data presented in this section are averaged both in time and in the two homogenous directions. The statistical data were gathered during a time period $t^+ = tu_{\tau i}^2/\nu_b = 1020$ (wall units) after a statistical steady solution was obtained. The results are normalised with the interfacial friction velocity $u_{\tau i}$ and the bulk fluid viscosity ν_b. In the following the interface corresponds to $y^+ = 0$ and the centre of the channel is at $y^+ \approx 165$.

The profile of mean streamwise velocity relative to the interface, $U^+ - U^+_{interface}$, is shown in fig. 6. The "law-of-the-wall" and the mean velocity profile from a conventional channel flow (Kim *et al.*, 1987) are also included for comparison. Close to the interface the mean velocity is clearly linear ($U^+ = y^+$) and similar to that in the near interface region

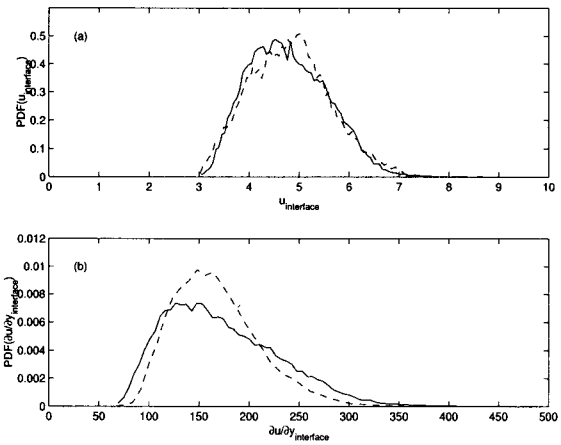

Figure 4: Probability density functions of (a) $u_{interface}$ and (b) $\partial u/\partial y_{interface}$. —, present simualtion; - - -, Solbakken *et al.* (2002).

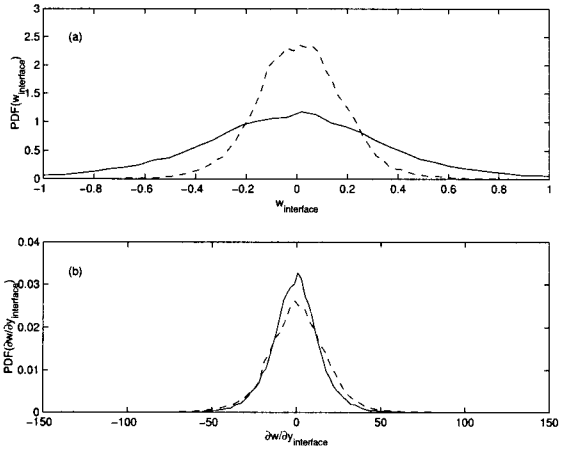

Figure 5: Probability density functions of (a) $w_{interface}$ and (b) $\partial w/\partial y_{interface}$. —, present simualtion; - - -, Solbakken *et al.* (2002).

in Solbakken *et al.* (2002). However, the mean velocity relative to the interfacial velocity is significantly lower than in Solbakken *et al.* (2002) in the logarithmic region. This deviation presumably arises due to the difference in turbulence intensities and Reynolds shear stress (to be shown later).

Figure 7(a) shows the root-mean-square (rms) velocity fluctuations u_{rms}, v_{rms} and w_{rms}, commonly referred to as turbulence intensities, from the interface to the centre of the channel. The region of the flow from $y^+ \approx 10$ and further off from the interface show a very similar behaviour as in Solbakken *et al.* (2002), and a perfect match between the two data-sets can be observed from $y^+ \approx 40$. The rms-values in the very-near interface region do on the other hand differ considerably. All tree components show an increase in turbulence activity close to the interface. The streamwise and wall-normal components, u_{rms} and v_{rms}, are both a bit too high and this will probably affect the Reynolds shear-stress $-\overline{uv}$. But the most obvious deviation is the spanwise component, w_{rms}, which is far too large in the present investigation. This is, as mentioned earlier, associated with the probability density function of $w_{interface}$ in fig. 5(a) which revealed a too large spreading of the spanwise interfacial velocity distribution. This is in turn probably related to the slope of eq. (3) which is too small, as can be seen from fig. 3.

Turning now to the Reynolds shear stress $-\overline{uv}$ plotted in fig. 7(b), the present distribution closely resembles that of Solbakken *et al.* (2002), but the near-interface region reveals a somewhat larger value of $-\overline{uv}$. This is as mentioned earlier due to the larger streamwise and wall-normal velocity fluctuations present close to the interface. This increase in Reynolds shear stress will directly affect the mean streamwise velocity gradient through the following relation for the total mean shear stress across the channel, $\tau_{total} = \mu dU/dy - \rho\overline{uv}$, which is a function of y only. The velocity gradient is therefore altered in the buffer region, resulting in a lower mean velocity in the logarithmic region (fig. 6) as compared to Solbakken *et al.* (2002).

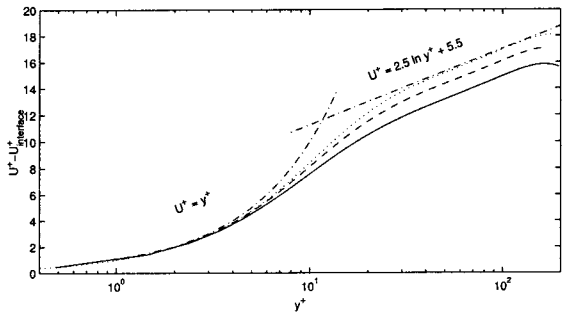

Figure 6: Mean streamwise velocity in the bulk flow. —, present simulation; - - -, Solbakken *et al.* (2002); ···, Kim *et al.* (1987); · — · — ·, "Law-of-the-wall".

Root-mean-square vorticity fluctuations normalised with $\nu_b/u_{\tau i}^2$ are presented in fig. 8. All three components show good agreement with data from Solbakken *et al.* (2002), except in the region very close to the interface ($y^+ \approx 0 \ldots 15$) where small differences exist. It is generally accepted that the streamwise vorticity ω_x in near-wall regions partly is a kinematic consequence of near-wall vortical structures primarily oriented in the streamwise direction and the no-slip boundary condition at the wall. This mechanism will also apply for the lubricated channel if the film is sufficiently thin. The location of maximum $\omega_{x,rms}$ at $y^+ \approx 18$, which is similar to Solbakken *et al.* (2002), corresponds to the average location of the centre of the streamwise vortices. This is also in close agreement with Kim *et al.* (1987) and their conventional channel flow, for which maximum streamwise vorticity at $y^+ \approx 20$ was reported. The increase of $\omega_{y,rms}$ near the interface is due to the somewhat larger turbulence intensities in the streamwise (u_{rms}) and spanwise (w_{rms}) directions (see fig. 7). The spanwise component of the vorticity fluctuations $\omega_{z,rms}$ is heavily overpredicted in the immediate vicinity of the interface ($y^+ \approx 0 \ldots 3$). This behaviour can be ascribed to the probability density function (PDF) of $\partial u/\partial y_{interface}$ in fig. 4(b), which shows a too widespread distribution. The value of $\omega_{z,rms}$ at the interface is almost equal to corresponding results close to a rigid wall (Kim *et al.*, 1987) where a value of 0.36 was reported.

COHERENT STRUCTURES

In order to investigate whether the proposed set of slip-flow boundary conditions, eqs. (2) and (3), is able to mimic interfacial motions capable of producing realistic instantaneous events, the focus of attention is now shifted towards the coherent vortical structures in the near-interface region.

The λ_2-vortex definition of Jeong and Hussain (1995) is adopted to capture vortical structures in the flow fields. A vortex core is defined as a connected region of negative λ_2, which is the second largest eigenvalue of the tensor

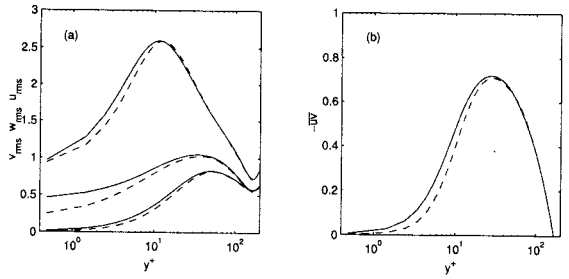

Figure 7: (a) Turbulence intensities and (b) Reynolds shear stress in the bulk flow. —, present simulation; - - -, Solbakken *et al.* (2002).

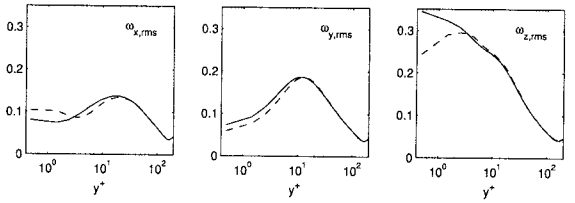

Figure 8: Root-mean-square vorticity fluctuations in the bulk flow. —, present simulation; - - -, Solbakken *et al.* (2002).

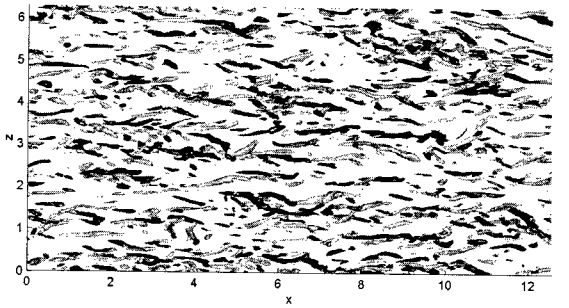

Figure 9: Isosurface plot of $\lambda_2 = -0.01$ in the region $0 < y^+ < 60$. Dark (light) shading represents positive (negative) streamwise vorticity ω_x.

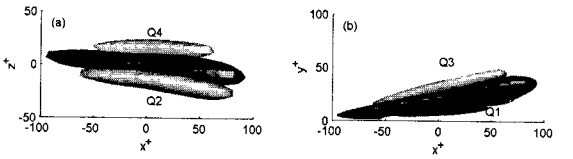

Figure 10: Isosurface plots of the ensemble-averaged coherent structure with positive ω_x. Dark shading represents $\lambda_2(\langle\vec{u}\rangle)$, while light shading represents the associated coherent Reynolds shear stress $-\langle u-U\rangle\langle v\rangle$. (a) top view, (b) side view.

$s_{ik}s_{kj} + r_{ik}r_{kj}$ where $s_{ij} = (u_{i,j} + u_{j,i})/2$ is the strain rate tensor and $r_{ij} = (u_{i,j} - u_{j,i})/2$ is the rotation tensor. Jeong *et al.* (1997) showed that this vortex definition is fully able to identify vortices in a turbulent channel flow. This definition essentially captures the pressure minimum in a plane perpendicular to the vortex axis, and also accurately identifies vortex cores in regions with high shear, contrary to vorticity-based vortex definitions. Figure 9 shows an instantaneous plot of isosurfaces of $\lambda_2 = -0.01$ in the region $0 < y^+ < 60$ (note that λ_2 is normalised with $\nu_b^2/u_{\tau i}^4$). This isosurface plot shows elongated structures nearly aligned in the streamwise direction. Both the streamwise extent and

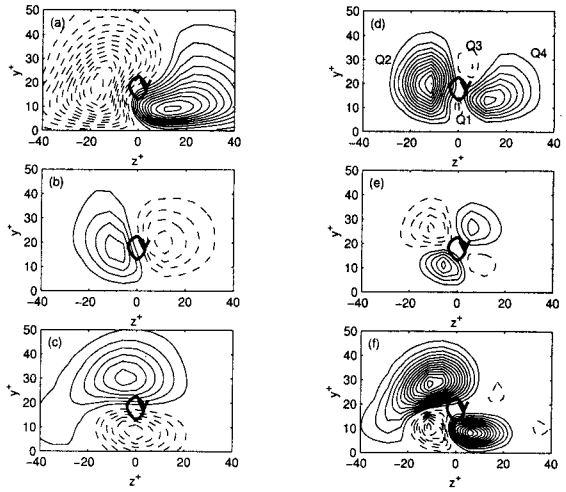

Figure 11: Ensemble-averaged coherent velocity fluctuations and Reynolds shear stresses. Positive and negative contours are represented by solid and broken lines, respectively. Contour increment 0.25. (a) $\langle u-U\rangle$, (b) $\langle v\rangle$, (c) $\langle w\rangle$, (d) $-\langle u-U\rangle\langle v\rangle$, (e) $-\langle v\rangle\langle w\rangle$, (f) $-\langle u-U\rangle\langle w\rangle$.

the tilting angles seem to correspond closely to the structures studied in Solbakken *et al.* (2002), and also to earlier observations close to rigid walls (Jeong *et al.* 1997). Dark (light) shading shows vortices with positive (negative) streamwise vorticity ω_x. Vortices with different sign of streamwise vorticity are known to be equally probable and are also symmetric counterparts (Jeong *et al.* 1997). This investigation is accordingly limited to only those vortices with positive streamwise vorticity.

In order to further study the near-interface quasi-streamwise vortices, an ensemble-averaging of the flow field around the vortices present in the instantaneous flow is performed. The detection and averaging are based on the scheme devised by Jeong *et al.* (1997) to identify coherent vortices in the near-wall region in a turbulent channel flow. The procedure consists of three steps: (I) Detection of vortical structures by the λ_2-definition conditioned on positive streamwise vorticity ω_x. (II) Ensemble-averaging of the structures by aligning the midpoint of their streamwise length. In order to capture only fully grown structures the structures are required to have a streamwise length of at least $x^+ = 150$ in the region $10 < y^+ < 40$. (III) Shifting of the alignment point to maximise the cross-correlation between the ensemble-averaged and the individual structures. Structures having a cross-correlation below 0.5 were discarded in order to reduce the smearing of the resulting coherent structure. The resulting ensemble-averaged field consists of coherent motions and is thus suitable as a generic model for the streamwise vortices.

In the following presentation the origin $(x^+, z^+) = (0, 0)$ in the plane parallel to the interface is defined to be the alignment point (midpoint of the structure). The ensemble average is based on a database consisting of 25 instantaneous flow fields separated in time by $\Delta t^+ = 40.8$. The ensemble eventually consists of 223 instantaneous structures. The brackets $\langle\rangle$ indicate ensemble-averaged quantities, and $\lambda_2(\langle\vec{u}\rangle)$ means that λ_2 is calculated from the averaged field.

Figure 10 shows an isosurface plot of λ_2 calculated from the ensemble-averaged field together with the associated coherent Reynolds shear stress $-\langle u-U\rangle\langle v\rangle$. The coherent field reveals a highly elongated quasi-streamwise vortex, inclined 10° in the vertical $(x-y)$-plane and tilted 6° in the hor-

izontal $(x-z)$-plane, whereas the corresponding ensemble averaged structure in Solbakken *et al.* (2002) was inclined 9° and tilted 7°. The streamwise extent of the structure is about 200 wall units, and it is evident that the coherent structure produces stronger ejections ($Q2$) than sweeps ($Q4$).

The coherent velocities and coherent Reynolds shear stresses in the $(y-z)$-plane through the midpoint ($x^+ = 0$) of the ensemble-averaged structure in fig. 10 are shown in fig. 11. The thick solid line is a contour of $\lambda_2(\langle\vec{u}\rangle)$ indicating the position of the centre of the structure and the arrow head shows the sense of rotation. The centre of the structure is located at $y^+ \approx 18$, which is about the same as in Solbakken *et al.* (2002) and about $\Delta y^+ = 5$ lower than in Jeong *et al.* (1997) close to a rigid wall. The streamwise $\langle u - U\rangle$ and spanwise $\langle w\rangle$ coherent velocity fluctuations in fig. 11(a) and (c) penetrate inside the lubricating film, a feature that was also reported by Solbakken *et al.* (2002). This is obviously not the case for the wall-normal component $\langle v\rangle$ in fig. 11(b) since the interface is impermeable. Figure 11(d) shows the coherent primary Reynolds shear stress $-\langle u - U\rangle\langle v\rangle$ which is the only shear stress component that produces a non-zero spatial average. It is positive nearly everywhere and the contribution from ejection events ($Q2$) is slightly larger than the contribution from sweep events ($Q4$). Small regions of negative $-\langle u - U\rangle\langle v\rangle$ ($Q1$ and $Q3$ events) occur above and below the structure centre, but these contribute only modestly to the Reynolds-averaged shear stress $-\overline{uv}$. All these features were also reported by Solbakken *et al.* (2002). The usual cloverleaf pattern can moreover be seen in fig. 11(e) for $-\langle v\rangle\langle w\rangle$. In fig. 11(f) the contours of $-\langle u - U\rangle\langle w\rangle$ also bear a close resemblance to Solbakken *et al.* (2002).

SUMMARY AND CONCLUDING REMARKS

A direct numerical simulation (DNS) of a lubricated channel flow where the lubricating film is replaced by a set of slip-flow boundary conditions is performed. The set of slip-flow boundary conditions is applied at the film-fluid interface and is supposed to mimic real interfacial motion. The boundary condition in the streamwise direction was derived by Joseph (1980) and describes a relation between the velocity and the velocity gradient at the interface. A similar slip-flow boundary condition is proposed for the spanwise direction. The simulation using the proposed boundary conditions compares satisfactorily with the full simulation by Solbakken *et al.* (2002) where both the lubricating film and the bulk fluid were solved within the DNS approach.

Probability density functions are constructed for the interfacial velocities and interfacial velocity gradients. All distributions, except for the spanwise velocity distribution, are well reproduced by the proposed slip-flow boundary conditions. The streamwise mean velocity is slightly underpredicted, which is probably an effect of too large interfacial velocity fluctuations and thereby an overestimation of the Reynolds shear stress close to the interface. In spite of the constraints on the interfacial motion imposed by the slip-flow conditions (2) and (3), near-wall vortical structures, both instantaneous and ensemble-averaged, are surprisingly similar to those deduced by Solbakken *et al.* (2002) from their full simualtion.

The present investigation has demonstrated that the presence of thin lubricating films can be accounted for by a set of dynamic slip-flow boundary conditions in numerical simulation of turbulent flows. The streamwise slip-flow boundary condition derived by Joseph (1980) reproduced streamwise interfacial velocities and velocity gradients very well. The proposed spanwise slip-flow boundary condition led to a somewhat too wide distribution of the spanwise velocity fluctuations. An obvious remedy would be to introduce a multiplicative factor of say 2.0, on the right-hand side of eq. (3). Nevertheless, the rather simple set of dynamic slip-flow conditions (2) and (3) have proved to assure the essential dynamics of the near-interfacial fluid motions so that even the characteristic coherent flow structures are properly developed.

ACKNOWLEDGEMENTS

This work has received support from The Research Council of Norway (Programme for Supercomputing) through a grant of computing time. The MGLET code was generously made available by Prof. H. Wengle (Universität der Bundeswehr München) and Prof. R. Friedrich (Technische Universität München).

REFERENCES

Beavers, B.V., and Joseph, D.D. (1967) Boundary condition at a naturally permeable wall. *J. Fluid Mech.* **30**, 197-207.

Gad-el-Hak, M. (1999) The fluid mechanics of microdevices - the Freeman scholar lecture. *J. Fluids Eng.* **121**, 5-33.

Greenspan, H.P. (1978) On the motion of a small viscous droplet that wets a surface. *J. Fluid Mech.* **84**, 125-143.

Hahn, S., Je, J., and Choi, H. (2002) Direct numerical simulation of turbulent channel flow with permeable walls. *J. Fluid Mech.* **450**, 259-285.

Jeong, J., and Hussain, F. (1995) On the identification of a vortex. *J. Fluid Mech.* **285**, 69-94.

Jeong, J., Hussain, F., Schoppa, W., and Kim, J. (1997) Coherent structures near the wall in a turbulent channel flow. *J. Fluid Mech.* **332**, 185-214.

Joseph, D.D. (1980) Boundary conditions for thin lubrication layers. *Phys. Fluids* **23**, 2356-2358.

Kim, J., Moin, P., and Moser, R. (1987) Turbulence statistics in fully developed channel flow at low Reynolds number. *J. Fluid Mech.* **177**, 133-166.

Manhart, M., Tremblay, F., and Friedrich, R. (2001) MGLET: a parallel code for efficient DNS and LES of complex geometries. in: *Parallel Computational Fluid Dynamics - Trends and Applications*, Elsevier, 449-456.

Miksis, M.J., and Davis, S.H. (1994) Slip over rough and coated surfaces. *J. Fluid Mech.* **273**, 125-139.

Navier, C.L.M.H. (1823) Mémoire sur les lois du mouvement des fluides. *Mémoires de l'Académie Royale des Sciences de l'Institut de France* **VI**, 389-440.

Orellano, A., and Wengle, H. (2000) Numerical simulation (DNS and LES) of manipulated turbulent boundary layer flow over a surface-mounted fence. *Eur. J. Mech. B-Fluids* **19**, 765-788.

Scardovelli, R., and Zaleski, S. (1999) Direct numerical simulation of free-surface and interfacial flow. *Annu. Rev. Fluid Mech.* **31**, 567-603.

Solbakken, S., Andersson, H.I., and Fontaine, E. (2002) Coherent structures in interfacial turbulence. in: *Advances in Turbulence IX - Proceedings of the Ninth European Turbulence Conference*, CIMNE, 429-432.